





Impact in granular matter: Force at the base of a container made with one movable wall

L. A. Torres Cisneros ^{1,*}, V. Marzulli ^{1,†}, C. R. K. Windows-Yule ² and T. Pöschel ^{1,‡}

¹*Institute for Multiscale Simulation, Friedrich-Alexander-Universität Erlangen-Nürnberg, Cauerstrasse 3, 91058 Erlangen, Germany*

²*School of Chemical Engineering, University of Birmingham, Edgbaston, Birmingham B15 2TT, United Kingdom*



(Received 24 February 2020; accepted 11 June 2020; published 14 July 2020; corrected 23 July 2020)

In geotechnics as well as in planetary science, it is important to find a means by which to protect a base from impacts of micrometeoroids. In the moon, for example, covering a moon base with regolith, and housing such regolith by movable bounding walls, could work as a stress-leaking shield. Using a numerical model, by performing impacts on a granular material housed in a rectangular container made with one movable sidewall, it is found that such wall mobility serves as a good means for controlling the maximum force exerted at the container's base. We show that the force exerted at the container's base decreases as the movable wall decreases in mass, and it follows a Janssen-like trend. Moreover, by making use of a dynamically defined redirecting coefficient $K(X)$, proposed by Windows-Yule *et al.* [*Phys. Rev. E* **100**, 022902 (2019)], which depends on the container's width X , we propose a model for predicting the maxima measured at the container's base. The model depends on the projectile and granulate properties, and the container's geometry.

DOI: [10.1103/PhysRevE.102.012903](https://doi.org/10.1103/PhysRevE.102.012903)

I. INTRODUCTION

The impact of a solid projectile onto a granulate is a well-known phenomenon in the physics of granular materials as well as in planetary science. For instance, in order to understand how the projectile moves into the granulate, some models have been proposed looking for the right projectile's equation of motion [1–11]. Some other studies were mainly focused on the propagation through the bulk of the shock wave created during an impact [12–15]. Besides, in planetary science, the features of the crater formed in an impact process have been studied in order to figure out the nature of the projectile [10,16–19]. Despite the above relevant studies on impacts, when a granular material is housed in a container, the role of the force acting on the container boundaries during an impact process is in many cases omitted. Furthermore, the evolution of such force when the granular material has been housed in a container whose geometry can be modified could help us to understand how the force acting on the base can be tuned. In this way, the present research has been addressed in order to look for a model for predicting the maximum force exerted at the container's base during an impact process, when it is made with a wall that could move because of the forces acting on it.

Nowadays, one important implication of such research concerns the determination of a means by which to protect a moon base from impacts of micrometeoroids. An option for a moon-base design suggests that the base must be protected by a granulate composed of lunar regolith in turn retained by movable bounding walls [20–23], as is shown in Fig. 1. It is important to remark that, in such a model, two particular

features should be taken into account: (i) the lunar regolith has been housed in a container made with movable bounding walls, and (ii) during an impact, the granulate experiences a compression.

A. A granulate housed in a container

Inside a granulate housed in a container, the loading forces are mainly carried by force chains [24–26]. These force chains redirect part of the granulate's weight toward any bounding wall because of its geometry and friction [27–29]. This gives rise to a Janssen-like force F , measured at the container's base, given by

$$F \propto 1 - e^{-\mu K \frac{P}{A} Z}, \quad (1)$$

where μ is the effective friction between the granulate and the container's wall, and P , A , and Z are the container's perimeter, base area, and filling height, respectively [27–30]. K is called a redirecting coefficient, and it satisfies the relationship $\sigma_{\text{wall}} = K\sigma_{\text{base}}$, where σ_i is the stress at the base or at the wall [30]. Equation (1) is obtained by modeling a continuum fluid whose frictional interaction with the surrounding walls causes an effective force that affects the weight of the granular material. Most of the time this force is directed upward. Recently, a reverse Janssen effect was found that causes an effective force pointing downward [31]. When this effective force points upward, it increases with the liquid's depth, Z , until a certain threshold is reached. For larger depth, the Janssen force saturates. The increase and saturation of the upward force results in a reduction of the granulate's apparent weight measured at the container base.

Furthermore, the force chains in a granulate change significantly along with the container's geometry, since such changing modifies grain-wall contacts [32]. In fact, it was shown recently by Windows-Yule *et al.* [33] that, in a container whose geometry changes at different rates, K becomes

*luis.torres@fau.de

†valentina.marzulli@fau.de

‡thorsten.poeschel@fau.de

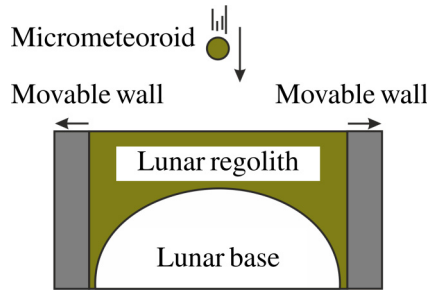


FIG. 1. Simple sketch of a moon base protected by a granulate composed by lunar regolith retained by movable bounding walls.

a function of such geometry [i.e., $K = K(X)$, where X is the container's width]. Thus, in order to understand the particular role played by the bounding movable walls during an impact, a simplified model, in comparison with the one shown in Fig. 1, is necessary. To isolate the desired scheme, we proposed a simpler model in which a granular material is housed within a rectangular container made with one movable wall, as is shown in Fig. 2.

B. A granulate under compression

It is found in granular materials that given the nonuniform grain-grain compression in each force chain, anomalous instantaneous stress distributions appear [24–26,29]. Then, when compressed, such grain-grain interaction yields a bulk force dependence of the form

$$F = E^* \Delta^\beta, \quad (2)$$

where E^* is the effective Young's modulus [15], Δ is the bulk compression, and $\beta > 1$ [15,34,35]. It has been shown by Clark *et al.* [15] (see the Appendix in this reference) that there are some circumstances in which, during an impact process, the mechanical response of the granulate, when slowly compressed, can be matched to the response of the material to a sudden impact. Moreover, Marzulli *et al.* [36] have recently shown that, by applying a punctual impulsive force on a granulate, while changing the width of the container, it is possible to model an impact process. This has been done by means of a finite-element analysis calibrated with data obtained from a discrete element analysis.

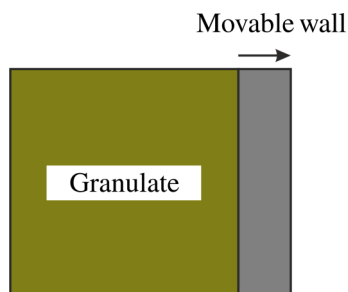


FIG. 2. Simplified model of the container made with one movable wall.

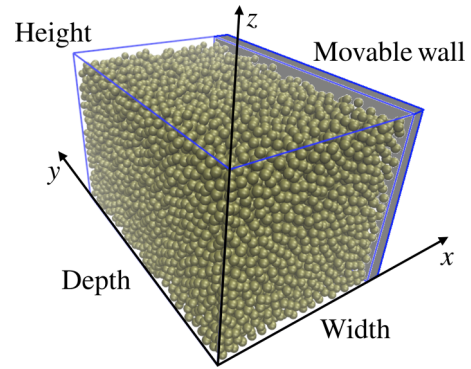


FIG. 3. Rectangular container made with one movable wall and filled with a granular material.

C. Aim

Taking into account the properties of a granular material, when housed in a container and when compressed, by means of discrete element method simulations, the present research was aimed at a model to predict the maximum force exerted at the container's base during an impact process, when it possesses one sidewall able to be moved by the forces acting on it.

II. METHODS

A. System description

The simulated system consists of a rectangular container made with five smooth walls (four sidewalls and the base), open from the top, filled with a granulate made of a polydisperse sample of spherical particles, as is shown in Fig. 3.

The container has a width $X_0 = 0.1$ m, a depth $Y_0 = 0.16$ m, and a height $Z_0 = 0.1$ m. The width, depth, and height were taken in the x , y , and z positive axes, respectively. The farthest wall in the x axis is taken as the movable one. Its movement is fully determined by the outward pressure exerted by the granular material, by the friction between the wall and the base, and by its mass M_w . The set of M_w used is written in Table I. The particles used in each sample have a radius ranging from $r_{\min} = 2.0$ mm to $r_{\max} = 3.0$ mm, with a uniform size distribution and a density $\rho = 1130$ kg/m³, while the total amount of grains N is equal to 12 568. The density of the particles has been chosen in order to simulate nylon beads.

TABLE I. Set of values used for M_w in kilograms.

0.2606	0.3165	0.5819
0.27	0.3212	0.6982
0.2793	0.3258	0.8146
0.2839	0.3305	0.931
0.2886	0.3351	1.0474
0.2932	0.3398	1.3966
0.2979	0.3444	2.0948
0.3025	0.3491	2.7931
0.3119	0.4655	3.4914

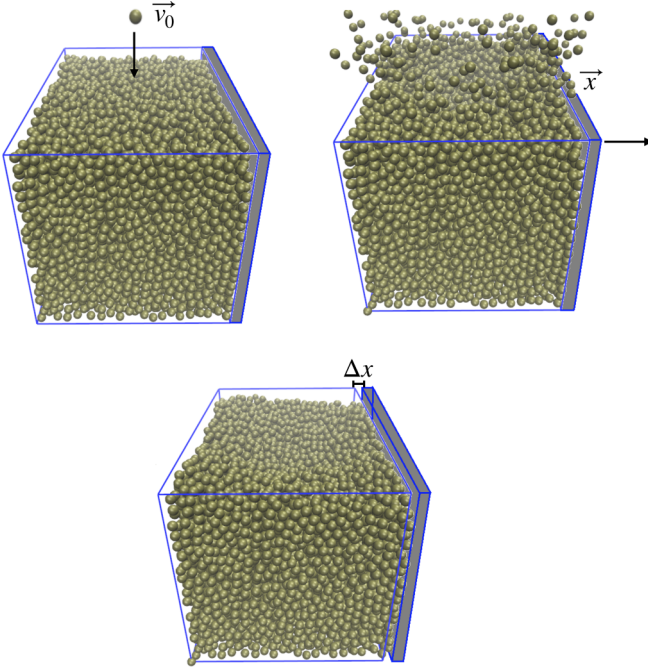


FIG. 4. Snapshots of the impact process. Shown is the system before (top image), during, and after the impact (lower left and right images, respectively).

To reproduce an impact after the container had been filled, a spherical projectile was dropped vertically (along the z axis) from a height $h_0 = 0.2$ m right in the center of the container with a given initial velocity v_0 . A set of four initial velocities $v_0 = \{\frac{10}{\sqrt{8}}, \frac{10}{\sqrt{4}}, \frac{10}{\sqrt{2}}, 10\}$ m/s has been implemented. The projectile has a radius $r_p = 5$ mm and a density $\rho_p = 7850$ kg/m³. Its density has been chosen in order to simulate a steel bead. Figure 4 shows a series of snapshots taken from one simulation describing the impact process.

Finally, the time in which the whole process (i.e., container filling and impact) had been simulated is of the order of 5 s of real time.

B. Preparation of the initial state

In the initial filling, all the particles are arranged randomly upward from the bottom of the container without overlapping, as is shown in Fig. 5, before being dropped vertically driven by the terrestrial gravity conditions ($g = 9.8$ m/s²).

During the filling all the lateral walls are completely fixed, and when the filling process is complete the movable wall is released. As already stated, the movement of this wall is determined by the outward pressure exerted by the granular material, by the friction between the wall and the base, and by its mass. Thus, the wall moves until the mechanical equilibrium between the granular material and the container is reached. At this stage, all the systems have achieved the packing fraction $\phi \approx 0.557$. Allowing the movement of one lateral wall of the system represents the greater innovation of this study, since the mechanical behavior of the system is highly influenced by such an imposed condition, as will be shown later.

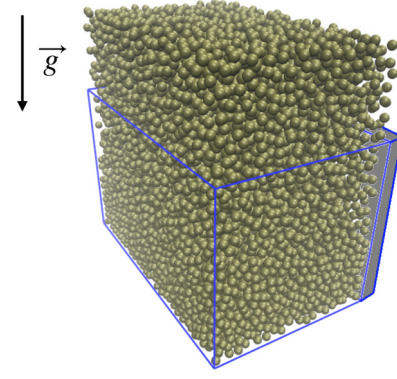


FIG. 5. Initial arrangement of the particles being pulled down by gravity.

C. Numerical method

To simulate an impact process, discrete element method simulations have been performed using MERCURYDPM software [37–39]. MERCURYDPM is a discrete element method integrator developed to simulate materials composed of a huge amount of macroscopic particles, where the main interactions between them are dissipative collisions and friction (i.e., granular materials), solving each equation of motion via a time-driven algorithm [40,41].

The model used in the present work to compute the normal force f_{ij}^n , exerted by the grain j on the grain i in a collision, is the linear spring-dashpot model [42], given by the equation

$$f_{ij}^n = \kappa \xi_{ij} + \gamma \dot{\xi}_{ij}, \quad (3)$$

where ξ_{ij} and $\dot{\xi}_{ij}$ are the relative compression and the relative rate of decompression between the grain j and the grain i , respectively. In the above model, the particle stiffness is modeled by the spring constant κ , and the damping constant is given by γ . In the present work, $\kappa_1 = 1.2 \times 10^5$ N/m has been implemented, and γ has been computed as

$$\gamma = -2m_{ij} \left(\frac{\ln(\epsilon)}{t_c} \right), \quad (4)$$

where m_{ij} is the reduced mass between the grain i and the grain j , defined as $m_{ij} = \frac{m_i m_j}{m_i + m_j}$. t_c is the time of collision and ϵ is the coefficient of restitution [42]. t_c has been set to 0.55×10^{-4} s, while $\epsilon = 0.9$.

To compute the friction f_{ij}^t between grains, Coulomb's law of friction [30] for the sliding case has been implemented, i.e., the force given by the friction satisfies the criterion

$$f_{ij}^t = \mu f_{ij}^n, \quad (5)$$

where μ is the coefficient of sliding friction, set to 0.25.

Furthermore, the time step implemented to solve the equations of motion has been imposed to be equal to $0.02 \times t_c$. The parameters used to compute the grain-wall and grain-projectile interactions are the same as those used to compute the grain-grain ones.

It is important to mention that for solving the wall's motion, since the force of friction is proportional to the coefficient of friction, an effective coefficient of friction $\mu^* = \eta M_w$

has been defined, where $\eta = 0.21 \text{ kg}^{-1}$, in order to set M_w as our control variable. In other words, the deceleration caused by the wall-base friction is computed by solving $\ddot{x} = \mu^*g$. In the present work, η has been chosen to give a friction $\mu = 0.58$ when $M_w = 2.7 \text{ kg}$.

D. Data analysis

When a container had been filled with granular material, it is well known that, given the presence of grain-grain and grain-wall friction, force chains will appear [24–26,29]. Such chains are in turn more (or less) stable as the boundaries are more (or less) static and rough [28,29,32]. If a projectile hits a container filled with a granulate, the force transmission will be driven by such force chains. Thus, any change in the system's boundary (during an impact) will modify the force transmitted by the projectile to the base.

Since the present work aims at understanding how the average stress at the container's base changes through an impact process, the net force at the base of the container F_{base} has been computed as a function of time. The net force is defined as

$$F_{\text{base}}(t) = \sum_{i=1}^{N_{\text{base}}} f_i, \quad (6)$$

where f_i is the projection of the normal force exerted by the base on the grain i , and N_{base} is the number of particles in touch instantaneously with the base. This has been done for the full set of wall masses M_w given in Table I, and for each initial velocity v_0 . Then, in order to understand the role played by the mobility of the wall, the maximum force experienced at the base $F_{\text{base}}^{\text{max}}$ during each impact process is plotted. As will be shown further, the mobility of the wall acts as a regulator of the maximum force transmitted to the base. It is easy to understand since such wall mobility works as a "leakage" of the stress transmission. As part of the stress leaks toward the movable wall, the force at the base decreases as the movable wall is more able to be pushed. Moreover, it is shown that, proposing a model that relies on Janssen's model principles [i.e., Eq. (1)] and using a dynamically defined K , as given in [33], it is possible to describe qualitatively the tendency followed by $F_{\text{base}}^{\text{max}}$ as a function of M_w , in a wide range of M_w .

It is found also that the general trend followed by $F_{\text{base}}^{\text{max}}(M_w)$ does not change when the projectile has been dropped with different initial velocities. Then, following a similar reasoning to that given in [15] (see the Appendix in this reference), and using an effectively static wall ($M_w = 3.49 \text{ kg}$), an empirical formula is proposed that relies on the impact velocity v like

$$F_{\text{base}}^{\text{max}}(v) = av^\alpha + W^* \quad (7)$$

to collapse all $F_{\text{base}}^{\text{max}}(M_w)$. Here a is a fit parameter related mainly to the bulk stiffness of the system at static conditions, and W^* is the apparent weight exerted by the granulate on the container's base when the projectile impinges onto the granulate's surface with an impact velocity close to zero.

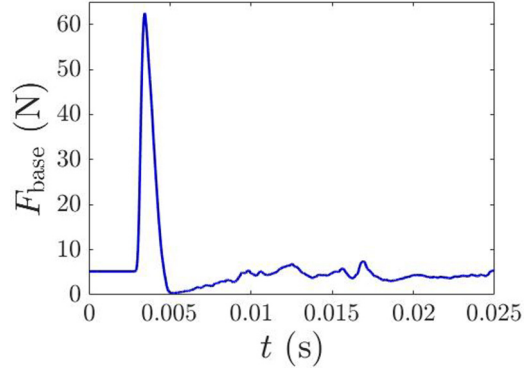


FIG. 6. Force exerted at the base F_{base} as a function of the time, for one single system composed by an effectively static wall ($M_w = 3.49 \text{ kg}$), during the impact of the projectile dropped with an initial velocity of 10 m/s.

III. RESULTS

A. Impact

The evolution of the impact process is plotted in Fig. 6 for one single system composed by an effectively infinite massive wall ($M_w = 3.49 \text{ kg}$) when the projectile has been dropped with an initial velocity $v_0 = 10 \text{ m/s}$. It can be observed that at the initial stage, about $t = 0 \text{ s}$, the force at the base remains constant with a value close to 5 N. This is because the base is experiencing the apparent weight W^* of the material. The apparent weight W^* is lower than the real weight of the material, which is instead equal to 9.87 N, because of the presence of the Janssen effect [27,29,30].

When the projectile hits the surface of the granulate, $F_{\text{base}}(t)$ increases until it achieves a maximum value of about 60 N. Previous experiments on impacts in unidimensional chains made of steel beads and two-dimensional photoelastic materials have been performed in Refs. [12,15]. These studies found similar values of the maximum force F_{base} in a range of impact velocities similar to those investigated in this study. Our results confirm that this maximum depends strongly on the impact velocity and on the granulate's bulk stiffness.

While the projectile is penetrating inside the granular material, the force experienced at the base starts to decrease. Surprisingly, the force decreases almost down to zero. This happens because the material touching the base reacts to the momentum transmitted by the projectile's impact, causing slight "levitation" of all the particles. Clearly, the presence of gravity pulls the material down again and it can be observed in the last plateau of the function, characterized also by tiny oscillations (Fig. 6). It is assumed that those tiny oscillations are related to the movement of the projectile inside the granulate, and to the rearrangement of the particles in the container.

To understand how the movement of one sidewall can influence F_{base} , the above process has been repeated for the full set of wall masses given in Table I. As is shown in Fig. 7(a), through the impact process all the systems described a similar trend, i.e., as the wall mass decreases the maximum peak of the force felt by the base decreases also. It suggests that the role of the wall's mobility is acting as a regulator of the stress transmitted.

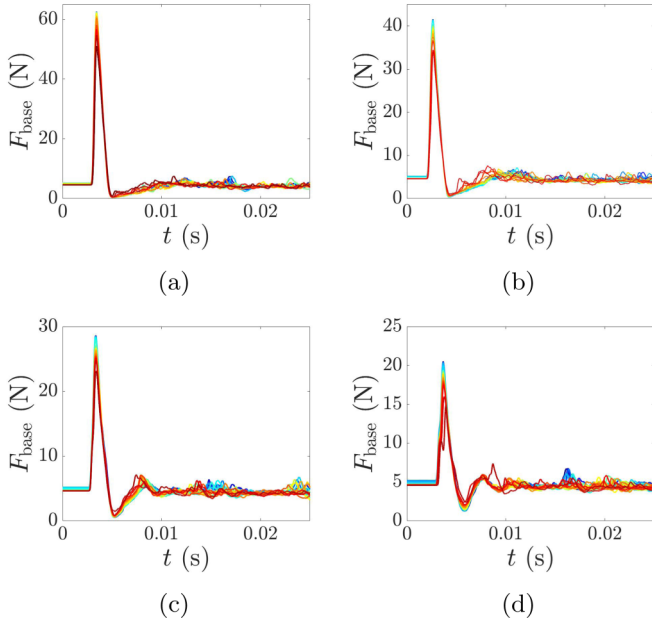


FIG. 7. Force exerted at the base as a time function, for the whole set of initial velocities. The initial velocities $v_0 = 10, 10/\sqrt{2}, 10/\sqrt{4}$, and $10/\sqrt{8}$ m/s belong to (a), (b), (c), and (d), respectively. M_w decreases from the blue color (largest mass) to the red one (lowest mass).

This decreasing of F_{base} when decreasing M_w could be explained by the following reasoning: When the projectile hits the granulate’s surface, a shock wave is created [15]. The speed of this shock wave is approximately two orders of magnitude faster than the projectile’s speed [15]. Thus, as soon as the projectile moves into the granulate’s upper layer, the shock wave impinges all the sidewalls. If the movable wall possesses more mass, the system could be seen as if all the walls were fixed. Then, this shock wave moves easily through the force chains in the granulate toward the base. On the other hand, when the movable wall possesses less mass, as soon as the shock wave reaches it, it will start to move slightly, leaking the stress transmitted to the base.

Repeating the same process for the full set of initial velocities v_0 [Figs. 7(b)–7(d)], it is found that, when the impact velocity decreases, the maximum force experienced at the base of the container sharply decreases as well. This can be understood since this maximum is mainly related to the changing of the projectile’s momentum: a greater change in the projectile’s momentum causes a larger peak of F_{base} . For all the impact velocities, a decreasing of the F_{base} ’s peak is always obtained by decreasing the mass of the wall also.

B. Maximum force

The main feature shown by each curve in Fig. 7 is the maximum reached by F_{base} . In Fig. 8, we plotted the maximum F_{base}^{max} as a function of M_w . It is easy to see that in all the curves, the mobility of the sidewall causes a leaking of the stress transmitted to the base, exhibiting a lower maximum when the wall possesses less mass (Fig. 8, red dots). Since all the curves describe a similar trend, there should be a specific dependence of F_{base}^{max} on the impact velocity v (the projectile’s

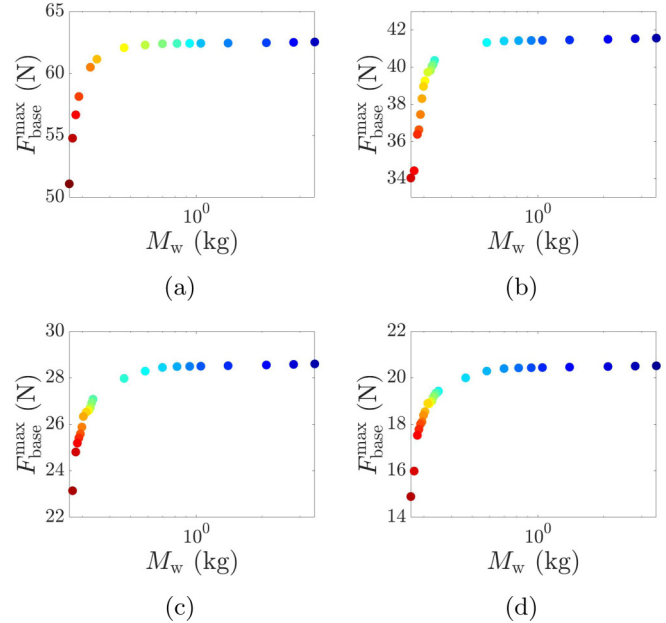


FIG. 8. Maximum F_{base} obtained as a function of M_w . The largest M_w corresponds to the blue color, while the lowest corresponds to the red one.

velocity right before it hits the granulate’s surface). It is clear that the impact velocity v is larger than the initial velocity v_0 since the projectile, once dropped from a certain height, is accelerated by gravity.

Looking for the right scaling between F_{base}^{max} and v , more simulations were performed to explore a wider range of impact velocities, keeping the system composed by an effectively static wall ($M_w = 3.49$ kg). The trend followed by $F_{base}^{max}(v)$ is shown in Fig. 9 (blue stars). The most notable mark is its nonlinear relation, which follows a noninteger power law. Proposing an empirical formula given by Eq. (7) and using the least-squares method, we find that the best fit gives $a = 2.49 \text{ N}/(\text{m/s})^\alpha$, $\alpha = 1.36$, and $W^* = 5.19 \text{ N}$ (Fig. 9, black curve). As previously mentioned, the value obtained in W^* is completely determined by the apparent

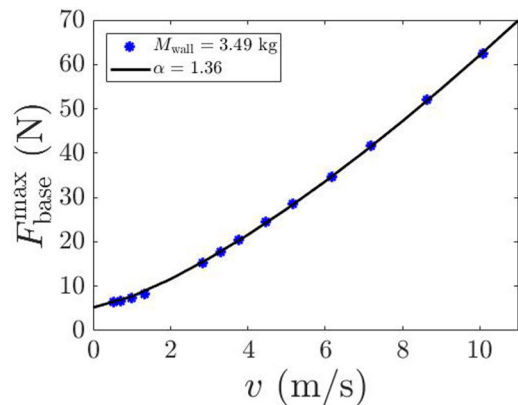


FIG. 9. Maximum force exerted at the base as a function of the impact velocity, for the system with $M_w = 3.49$ kg. The trend follows a power law with an exponent $\alpha = 1.36$.

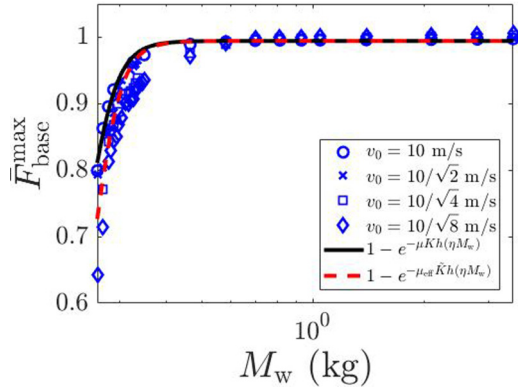


FIG. 10. Maximum force exerted at the base as a function of the mass of the movable wall divided by the fitting obtained in Eq. (7).

weight of the material when the projectile impinges onto the granulate's surface with a velocity close to zero. Hence W^* could be considered as the granulate's apparent weight. The role of a and α will be discussed in the Secs. IV B and IV C, respectively. Finally, this fitting allows us to collapse all the points plotted in Fig. 8 in a single trend shown in Fig. 10 (blue markers). Since we are collapsing the curves using the system with an effectively static wall, any other system experiences a larger stress at the base when a projectile hits its surface.

IV. DISCUSSION

A. Proposing a Janssen-like model

The role of the wall's mobility is important because it causes a stress-leaking effect. This leaking reduces the force exerted at the base since part of the stress wave moves toward the movable wall instead of the container's base. As the movable wall possesses less mass, it is more easily pushed, leaking a larger amount of stress. Otherwise, when the container is made with an effectively infinite massive wall, it behaves like a system made with completely fixed walls. Then, the stress wave moves easily through the force chains to the container's base causing a larger $F_{\text{base}}^{\text{max}}$.

To understand the trend shown by the blue markers in Fig. 10, we present the following reasoning: when a container filled with a granulate remains static, the stress measured at the base is given by Janssen's model [27,30],

$$\bar{F}_{\text{base}}^{\text{max}} = 1 - e^{-\mu K \frac{P}{A_{\text{base}}} Z}, \quad (8)$$

where we consider that $\bar{F}_{\text{base}}^{\text{max}}$ has been divided by any quantity multiplying the right side of the equation. In the case of rectangular containers, $P = 2(X + Y)$ and $A_{\text{base}} = XY$, where X and Y are the container's width and depth, respectively. Z is the container's filling height. In the present system, during the impact, the width of the container changes. Then, we can rewrite X as $X_0 + \Delta x$, where X_0 is the container's initial width and Δx is a small displacement. The numerical value of Δx is the maximum wall's displacement, which is a time-independent quantity. From numerical simulations, we obtained the dependence of Δx on the mass of the wall:

$$\Delta x = \Delta x_0 e^{-\zeta \eta M_w}. \quad (9)$$

Here ζ is a parameter mainly related to the quickness of the changing of the container's geometry, and Δx_0 is a fit parameter. Hence, we can rewrite X as

$$X(\eta M_w) = X_0 + \Delta x_0 e^{-\zeta \eta M_w}. \quad (10)$$

After the container's filling and before the impact, the container changes its width a bit until the mechanical equilibrium between the granulate and its container is reached. Such changing has been considered as an effective width given by Eq. (10). Now, it is possible to relate X with Z by assuming that, while the wall is being pushed away, the ZX area remains constant. Then, we get $A = ZX$. Therefore, replacing Z in Eq. (8), and considering $X(\eta M_w)$ as given by Eq. (10), we can rewrite Eq. (8) as

$$\bar{F}_{\text{base}}^{\text{max}} = 1 - e^{-\mu K h(\eta M_w)}, \quad (11)$$

where

$$h(\eta M_w) = 2A \frac{X + Y_0}{X^2 Y_0}. \quad (12)$$

Equation (11), which we call a "Janssen-like" model since we depart from the Janssen considerations [27,30], explains the decreasing of $F_{\text{base}}^{\text{max}}(M_w)$ as a process in which the stress-leaking effect is because of the changing of the container's geometry. Placing Eq. (10) in Eq. (8) and considering the product μK constant, as stated by Janssen's model [27,30], it is found that the best fit gives $\mu K = 1.59$, $\Delta x_0 = 29.8$ m, and $\zeta = 102.3$. As can be seen, in Fig. 10 (black solid curve) the present model describes quite well the tendency shown by the larger M_w . But at lower M_w , the model passes a bit above the blue markers. This happens mainly because the product μK has been assumed constant, and it should be understood that K depends strongly on the container's geometry.

To compute $\tilde{K}(X)$, which changes as the container's geometry does, we follow the reasoning given by Windows-Yule *et al.* [33] by defining

$$\tilde{K} = \frac{\mu K}{1 - e^{-\mu K h(\eta M_w)}} - \frac{1}{h(\eta M_w)}, \quad (13)$$

where μK is the same above-computed one, when considered constant. Moreover, we must multiply \tilde{K} by μ_{eff} in order to maintain the effect caused by the effective grain-wall friction, since Janssen's model makes use of both parameters. We can obtain this by computing $\mu_{\text{eff}} = \frac{\mu K}{\tilde{K}(\eta M_w)}$, where $M_w = 3.49$ kg. This gives $\mu_{\text{eff}} = 1.29$. As is shown in Fig. 10 (red dashed line), the trend given by using the product $\mu_{\text{eff}} \tilde{K}$, which depends on the container's geometry, still fits quite well the blue markers at larger M_w . When decreasing M_w , the model decays more quickly than that when considering μK constant, passing through more blue markers. This suggests that the role of a dynamically defined \tilde{K} is necessary in order to consider the effects caused by the changing of the container's geometry.

B. Dependence of a on the grain stiffness

The second fruitful result obtained is the fitting given by Eq. (7). It has been shown in previous experiments [34,35] that, when a granular material is compressed, the mechanical bulk's response follows a power law with noninteger

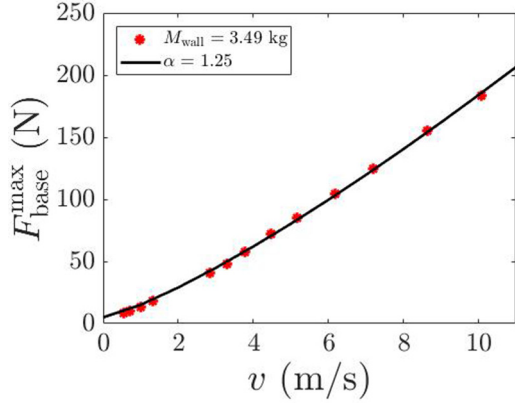


FIG. 11. Maximum force exerted at the base as a function of the impact velocity for a system made of stiffer particles ($\kappa_2 = 1.2 \times 10^6$ N/m). The fitting given in Eq. (7) gives an exponent $\alpha = 1.25$.

exponents of the form

$$F_{\text{base}}^{\text{max}} = E^* \Delta^\beta, \quad (14)$$

where Δ is the bulk compression, E^* is the effective Young's modulus [15] determined by the mechanical bulk properties of the system at static conditions, and β is the power-law dependence. To figure out the relationship between a and the mechanical response of the system to an impact, more simulations were performed with particles with a stiffness 10 times larger; $\kappa_2 = 10 \times \kappa_1$. As is shown in Fig. 11, although the trend is still well fitted by a power law, the values for the fitting are different. Values of $a = 10.11$ N/(m/s) $^\alpha$, $W^* = 4.97$ N, and $\alpha = 1.25$ have been obtained.

To understand the meaning of a and α , we can suppose that the impact process can be seen as two solid bodies colliding. Then, such a collision can be modeled by a nonlinear spring-mass system, where the mass is the mass of the projectile and the spring is the granular material reacting to an impact. In other words, the spring reacts following the relationship given by Eq. (14). Considering that the maximum achieved by F_{base} is mainly driven by the first shock wave, and the speed of this wave is about two orders of magnitude faster than the impact velocity, it could be assumed that this maximum is felt at the base before the dissipation because interparticle collisions start to play a role. By this reasoning, the conservation of energy could be applied. Then, we have the relationship

$$\frac{1}{2} \rho_p V_p v^2 = \frac{1}{1 + \beta} E^* \Delta^{1 + \beta}, \quad (15)$$

where ρ_p and V_p are the projectile's density and volume, respectively. Replacing Δ in Eq. (14), we have

$$F_{\text{base}}^{\text{max}}(v) = \left(\frac{E^{*\beta} (1 + \beta) \rho_p V_p}{2} \right)^{\beta / (1 + \beta)} v^{2\beta / (1 + \beta)}. \quad (16)$$

This equation is similar to that proposed in Eq. (7), where $a = \left(\frac{E^{*\beta} (1 + \beta) \rho_p V_p}{2} \right)^{\beta / (1 + \beta)}$ and $\alpha = 2\beta / (1 + \beta)$. In Eq. (7), the limit $v \rightarrow 0$ concerns the case in which the projectile impinges on the granulate with very small impact velocity, which causes a tiny perturbation in the system. This leads to a force measured at the base very close to W^* . With

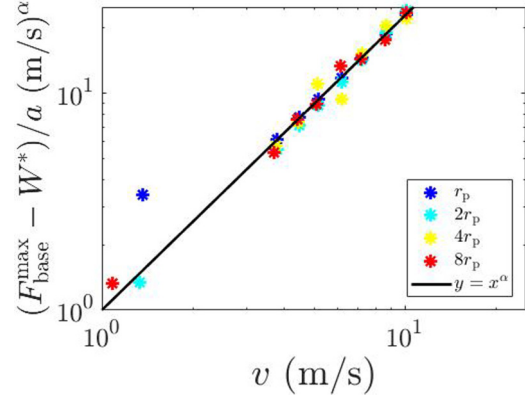


FIG. 12. Trend followed by $(F_{\text{base}}^{\text{max}} - W^*)/a$ as a function of v^α in a log-log scale for projectile radii ranging from $r_p = 5$ mm to $8r_p$ (color stars), and compared with a function $y = x^\alpha$ (solid black line), where $\alpha = 1.36$.

the above-obtained relationships, it is shown that a retains the mechanical properties of the material, being modified when the power-law changes, as well as the projectile ones. Following the above-obtained relationships, the equivalent values for $\alpha_1 = 1.36$ and $\alpha_2 = 1.25$ are $\beta_1 \approx 2.1$ and $\beta_2 \approx 1.6$, respectively. β_1 belongs to the system with less stiffness ($\kappa_1 = 1.2 \times 10^5$ N/m), and β_2 corresponds to that stiffer one ($\kappa_2 = 1.2 \times 10^6$ N/m). Then, the exponents α obtained in each fitting are explained by the fact that, when a granular system has been compressed, the mechanical bulk response deviates from a linear one, and this yields exponents $\beta > 1$ [15,34,35]. Furthermore, it has been shown in [15] that in a system composed by particles with a larger stiffness, β is larger than that obtained in a system composed by softer particles. This happens because in a system with less stiffness, the number of contacts between particles increases more quickly than in a stiffer system, causing a more uniform stress distribution [15,35].

C. Dependence of α on the projectile's size

Another important step done in order to approximate the interaction between the projectile and the granular material is the use of Eq. (15). Here such an interaction has been modeled as a nonlinear spring-mass system in which the energy is conserved by assuming that the first front-wave is what causes the largest maximum exhibited by $F_{\text{base}}^{\text{max}}(v)$. And this front-wave reaches the bottom faster than the dissipation of the energy because the interparticle collisions start to play a role.

One way to corroborate that such an approximation is valid is by looking at the changing of α in Eq. (7) when changing the projectile's size. If such an approximation were not valid, the assumption of an α independent of the projectile's size would also not be valid. Plotted in log-log scale in Fig. 12 is the trend followed by Eq. (7) by isolating v^α for different projectile sizes, and it is compared with a function $y = x^\alpha$, where $\alpha = 1.36$ (black solid line). As is shown, when varying the projectile's radii from r_p to $8r_p$, all the points fall into the same slope given by $\alpha = 1.36$. This corroborates that the above-found α does not depend on the projectile's size.

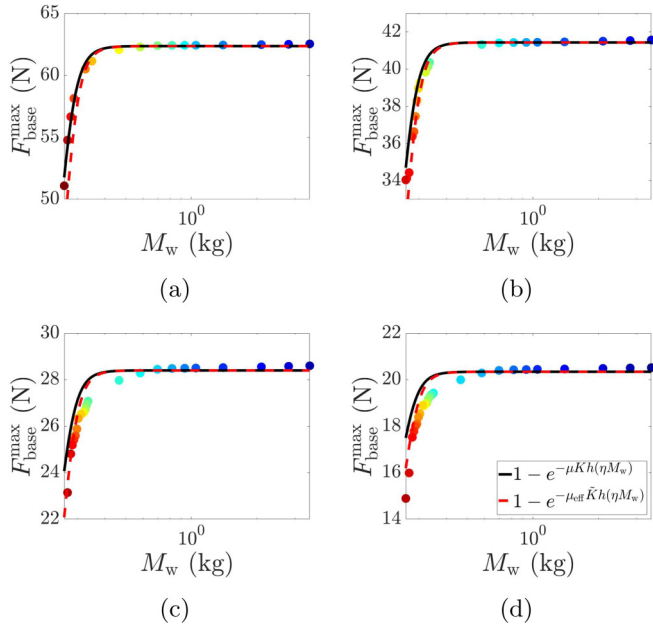


FIG. 13. Comparison between the trend obtained by using a model with a constant K (black solid line) and the one with a dynamic \tilde{K} (red dashed line), for each initial velocity v_0 .

D. A single master curve

Finally, Eqs. (7), (11), and (13) can be joined in a single master function as

$$F_{\text{base}}^{\text{max}}(M_w, v) = av^\alpha (1 - e^{-\mu_{\text{eff}} \tilde{K} h(\eta M_w)}) + W^*. \quad (17)$$

To show explicitly the “effectiveness” of this model, we plotted in Fig. 13 the trend obtained by using Eq. (17) with a constant K (black solid line) and with a width-dependent \tilde{K} (red dashed line), and we compared it to $F_{\text{base}}^{\text{max}}(M_w)$ for each initial velocity. As is shown, for larger M_w both

models fit similarly well $F_{\text{base}}^{\text{max}}$. When decreasing M_w , both models start to depart from each other; the best one has a “dynamically” defined \tilde{K} [Eq. (13)]. In the case of $v_0 = 10/\sqrt{4}$ and $10/\sqrt{8}$, the maxima shown between the yellow and the blue markers do not fall into the proposed model. This suggests that a could depend as well on the container’s geometry.

V. CONCLUSIONS

We investigated the ability of a granular material housed in a rectangular container, which is made with one movable sidewall, to tune the vertical transmission of the force from an impacting object to the container’s base. It is shown that such a system can indeed significantly reduce the force felt at the base, and that the magnitude of this force decreases monotonically as the mobility of the bounding wall increases. This observation has been explained in terms of a modified Janssen theory [33] for interpreting the container’s deformation as a source of leakage of the vertical force in the lateral directions. Building upon this theory and using the properties of granular materials when compressed during an impact [15], a detailed model is proposed from which the maximal force exerted at the base of our system may be predicted, taking into account the properties and incident velocity of a given projectile, the physical properties of the granular medium, and the mass (and thus mobility) of the bounding walls. This model not only provides valuable physical insight into the system of interest, but it may prove highly useful in the design and optimization of impact-mitigation systems, such as those currently being considered for the shielding of lunar habitations [20–23].

ACKNOWLEDGMENT

We acknowledge the support from Interdiziplinäres Zentrum für Nanostrukturierte Filme (IZNF) at FAU.

-
- [1] M. P. Ciamarra, A. H. Lara, A. T. Lee, D. I. Goldman, I. Vishik, and H. L. Swinney, Dynamics of Drag and Force Distributions for Projectile Impact in a Granular Medium, *Phys. Rev. Lett.* **92**, 194301 (2004).
 - [2] H. Katsuragi and D. J. Durian, Unified force law for granular impact cratering, *Nat. Phys.* **3**, 420 (2007).
 - [3] E. L. Nelson, H. Katsuragi, P. Mayor, and D. J. Durian, Projectile Interactions in Granular Impact Cratering, *Phys. Rev. Lett.* **101**, 068001 (2008).
 - [4] F. Pacheco-Vázquez, G. A. Caballero-Robledo, J. M. Solano-Altamirano, E. Altshuler, A. J. Batista-Leyva, and J. C. Ruiz-Suárez, Infinite Penetration of a Projectile into a Granular Medium, *Phys. Rev. Lett.* **106**, 218001 (2011).
 - [5] E. Altshuler, H. Torres, A. González-Pita, G. Sánchez-Colina, S. Waitukaitis, C. Pérez-Penichet, and R. C. Hidalgo, Settling into different granular media in different gravities, *Geophys. Res. Lett.* **41**, 3032 (2014).
 - [6] A. H. Clark, L. Kondic, and R. P. Behringer, Particle Scale Dynamics in Granular Impact, *Phys. Rev. Lett.* **109**, 238302 (2012).
 - [7] H. Katsuragi and D. J. Durian, Drag force scaling for penetration into granular media, *Phys. Rev. E* **87**, 052208 (2013).
 - [8] S. Joubaud, T. Homan, Y. Gasteuil, D. Lohse, and D. van der Meer, Forces encountered by a sphere during impact into sand, *Phys. Rev. E* **90**, 060201 (2014).
 - [9] C. S. Bester and R. P. Behringer, Collisional model of energy dissipation in three-dimensional granular impact, *Phys. Rev. E* **95**, 032906 (2017).
 - [10] D. van der Meer, Impact on granular beds, *Annu. Rev. Fluid Mech.* **49**, 463 (2017).
 - [11] N. Krizou and A. H. Clark, Power-Law Scaling of Early-Stage Forces During Granular Impact, *Phys. Rev. Lett.* **124**, 178002 (2020).
 - [12] V. F. Nesterenko, Solitary waves in discrete media with anomalous compressibility and similar to “sonic vacuum”, *J. Phys. IV* **4**, C8-729 (1994).
 - [13] C. Daraio, V. F. Nesterenko, E. B. Herbold, and S. Jin, Strongly nonlinear waves in a chain of teflon beads, *Phys. Rev. E* **72**, 016603 (2005).

- [14] L. R. Gómez, A. M. Turner, M. van Hecke, and V. Vitelli, Shocks Near Jamming, *Phys. Rev. Lett.* **108**, 058001 (2012).
- [15] A. H. Clark, A. J. Petersen, L. Kondic, and R. P. Behringer, Nonlinear Force Propagation During Granular Impact, *Phys. Rev. Lett.* **114**, 144502 (2015).
- [16] H. J. Melosh, *Impact Cratering: A Geologic Process* (Oxford University Press, Oxford, 1989).
- [17] J. C. Ruiz-Suárez, Penetration of projectiles into granular targets, *Rep. Prog. Phys.* **76**, 066601 (2013).
- [18] R. Bartali, Y. Nahmad-Molinari, and Gustavo M. Rodríguez-Liñán, Low Speed Granular-Granular Impact Crater Opening Mechanism in 2D Experiments, *Earth, Moon, and Planets* **116**, 115 (2015).
- [19] F. Pacheco-Vázquez, Ray Systems and Craters Generated by the Impact of Nonspherical Projectiles, *Phys. Rev. Lett.* **122**, 164501 (2019).
- [20] F. Ruess, J. Schänzlin, and H. Benaroya, Structural design of a lunar habitat, *J. Aerospace Eng.* **19**, 3 (2006).
- [21] H. Benaroya, *Turning Dust to Gold. Building a Future on the Moon and Mars* (Springer, Praxis, 2010).
- [22] G. Cesaretti, E. Dini, X. De Kestelier, V. Colla, and L. Pambaguian, Building components for an outpost on the lunar soil by means of a novel 3D printing technology, *Acta Astron.* **93**, 430 (2014).
- [23] F. Cafaro, E. Miticocchio, and V. Marzulli, Remarks on the reliability of physical modeling of lunar geotechnical structures, *Studia Geotech. Mech.* **40**, 133 (2018).
- [24] R. P. Behringer, D. Howell, L. Kondic, S. Tennakoon, and C. Veje, Predictability and granular materials, *Physica D* **133**, 1 (1999).
- [25] J. Geng, G. Reydellet, E. Clément, and R. P. Behringer, Green's function measurements of force transmission in 2D granular materials, *Physica D* **182**, 274 (2003).
- [26] K. E. Daniels, J. E. Kollmer, and J. G. Puckett, Photoelastic force measurements in granular materials, *Rev. Sci. Instrum.* **88**, 051808 (2017).
- [27] M. Sperl, Experiments on corn pressure in silo cells—Translation and comment of janssen's paper from 1895, *Granular Matter* **8**, 59 (2006).
- [28] M. Yasinul Karim and Eric I. Corwin, Eliminating Friction with Friction: 2D Janssen Effect in a Friction-Driven System, *Phys. Rev. Lett.* **112**, 188001 (2014).
- [29] R. Blanco-Rodríguez and G. Pérez-Ángel, Stress distributions in two-dimensional silos, *Phys. Rev. E* **97**, 012903 (2018).
- [30] J. Duran, A. Reisinger, and P. G. de Gennes, *Sands, Powders, and Grains: An Introduction to the Physics of Granular Materials, Partially Ordered Systems* (Springer, New York, 1999).
- [31] S. Mahajan, M. Tennenbaum, S. N. Park, D. Baxter, X. Fan, P. Padilla, A. Fernandez-Nieves, and M. P. Ciamarra, Reverse Janssen Effect in Narrow Granular Columns, *Phys. Rev. Lett.* **124**, 128002 (2020).
- [32] H. Pacheco-Martínez, H. J. van Gerner, and J. C. Ruiz-Suárez, Storage and discharge of a granular fluid, *Phys. Rev. E* **77**, 021303 (2008).
- [33] C. R. K. Windows-Yule, S. Mühlbauer, L. A. Torres Cisneros, P. Nair, V. Marzulli, and T. Pöschel, Janssen effect in dynamic particulate systems, *Phys. Rev. E* **100**, 022902 (2019).
- [34] T. Lachhab and C. Weill, Compression of a soft sphere packing, *Eur. Phys. J. B* **9**, 59 (1999).
- [35] N. Brodu, J. A. Dijksman, and R. P. Behringer, Spanning the scales of granular materials through microscopic force imaging, *Nat. Commun.* **6**, 6361 (2015).
- [36] V. Marzulli, L. A. Torres Cisneros, A. di Lernia, C. Robert, K. W. Yule, F. Cafaro, and T. Pöschel, Impact on granular bed: Validation of discrete element modeling results by means of two dimensional finite element analysis, *Granular Matter* **22**, 22 (2020).
- [37] A. R. Thornton, T. Weinhart, S. Luding, and O. Bokhove, Modeling of particles size segregation: Calibration using the discrete particle method, *Mod. Phys. C* **23**, 1240014 (2012).
- [38] T. Weinhart, A. R. Thornton, S. Luding, and O. Bokhove, From discrete particles to continuum fields near a boundary, *Granular Matter* **14**, 289 (2012).
- [39] T. Weinhart, L. Orefice, M. Post, M. P. van Schrojenstein Lantman, I. F. C. Denissen, D. R. Tunuguntla, J. M. F. Tsang, H. Cheng, M. Y. Shaheen, H. Shi, P. Rapino, E. Grannonio, N. Losacco, J. Barbosa, L. Jing, J. E. Alvarez Naranjo, S. Roy, W. K. den Otter, and A. R. Thornton, Fast, flexible particle simulations—An introduction to Mercury DPM, *Comput. Phys. Commun.* **249**, 107129 (2020).
- [40] T. Pöschel and T. Schwager, *Computational Granular Dynamics. Models and Algorithms* (Springer-Verlag, Berlin, 2005).
- [41] G. Pérez, Numerical simulations in granular matter: The discharge of 2D silo, *Pramana J. Phys.* **70**, 989 (2008).
- [42] J. Schäfer, S. Dippel, and D. E. Wolf, Force schemes in simulations of granular materials, *J. Phys. I France* **6**, 5 (1996).

Correction: The author list in Ref. [11] contained errors and has been fixed.